J Sol-Gel Sci Technol (2014) 71:333–341
DOI 10.1007/s10971-014-3383-8

ORIGINAL PAPER

Structure, optical and magnetic properties of $LaFeO_3$ nanoparticles prepared by polymerized complex method

Sumalin Phokha · Supree Pinitsoontorn · Santi Maensiri · Saroj Rujirawat

Received: 12 February 2014 / Accepted: 29 April 2014 / Published online: 9 May 2014

Abstract This work reports the study the structure, optical and magnetic properties of $LaFeO_3$ nanoparticles synthesized by the polymerized complex method. The $LaFeO_3$ nanoparticles were successfully obtained from calcination of the precursor at different temperatures from 750 to 1,050 °C in air for 2 h. The calcined $LaFeO_3$ nanoparticles were characterized by X-ray diffraction (XRD), transmission electron microscopy (TEM), UV–Visible spectroscopy, X-ray photoelectron spectroscopy (XPS), X-ray absorption near edge spectroscopy (XANES) and vibrating sample magnetometry. The XRD and TEM results showed that all $LaFeO_3$ samples had a single phase nature with the orthorhombic structure. The estimated crystallite sizes were in the range of 44.5 ± 2.4–74.1 ± 4.9 nm. UV–Vis spectra showed strong UV and Vis absorption with small band gap energy. The valence states of Fe ions were in the Fe^{3+} and Fe^{4+} state, as confirmed by XPS and XANES results. The weak ferromagnetic behavior with specific saturation magnetization of 0.1 emu/g at 10 kOe was obtained for the small particle of 44.5 ± 2.4 nm. The uncompensated spins at the surface was proposed as playing a part in the magnetic properties of small sized $LaFeO_3$.

Keywords $LaFeO_3$ · Nanoparticles · Magnetic properties · X-ray photoelectron spectroscopy (XPS) · X-ray absorption near edge spectroscopy (XANES)

S. Phokha (✉) · S. Maensiri · S. Rujirawat
School of Physics, Institute of Science, Suranaree University of Technology, Nakhon Ratchasima 30000, Thailand
e-mail: sumalinphokha@gmail.com

S. Pinitsoontorn
Department of Physics, Faculty of Science, Khon Kaen University, Khon Kaen 40002, Thailand

1 Introduction

$LaFeO_3$-type perovskite is one of the most important materials and has attracted attention because of their wide applications, such as electrodes materials for fuel cells, catalysts, chemical sensors, optoelectronic devices [1–5], etc. The substitution with various transition metal (TM) ions in the composition site is observed to improve the electrical/magnetic properties. In earlier report, $(Pb_{0.8}La_{0.2})(Ti_{0.8}Fe_{0.2})O_3$ sample originates from combining A-site (lone pair) ferroelectricity with B-site magnetic order among substitution at A-site and B-site. Results of detailed dielectric, ferroelectric, and magnetic studies are reported to show that the broad transitions in dielectric spectra correspond to the magnetic ordering in the sample [6]. Therefore, the incorporation of divalent or trivalent cations into the La or Fe sub-lattices has been major investigated as alternatives [6–8].

Recently, the magnetic properties of $LaFeO_3$ have been extensively studied but the magnetic study of $LaFeO_3$ nanoparticles is rare [9]. Antiferromagnetic nanoparticles always show unusual magnetic properties due to the finite-size effects, surface anisotropy effects, interface effects, shape anisotropy effect and so on [10–12]. In addition, the introduction of Ba^{2+} ions into La^{3+} site causes a decrease in the number of covalence bonds leads to the limitation of displacement in octahedron [13]. Moreover, mixed valences of $Fe^{3+}/Fe^{3+}/Fe^{4+}$ by oxygen non-stoichiometry of the materials were expected for improvement the magnetic property. Therefore, nano-size of $LaFeO_3$ system has been major investigated as an alternative. Various types of $LaFeO_3$ nanoparticles can be synthesized by many methods such as sol–gel [14–16], co-precipitation [17], bull milling [18], sonochemical [19], and hydrothermal [20].

Polymerized complex (PC) method has been synthesized on polyester network between citric acid (CA) and

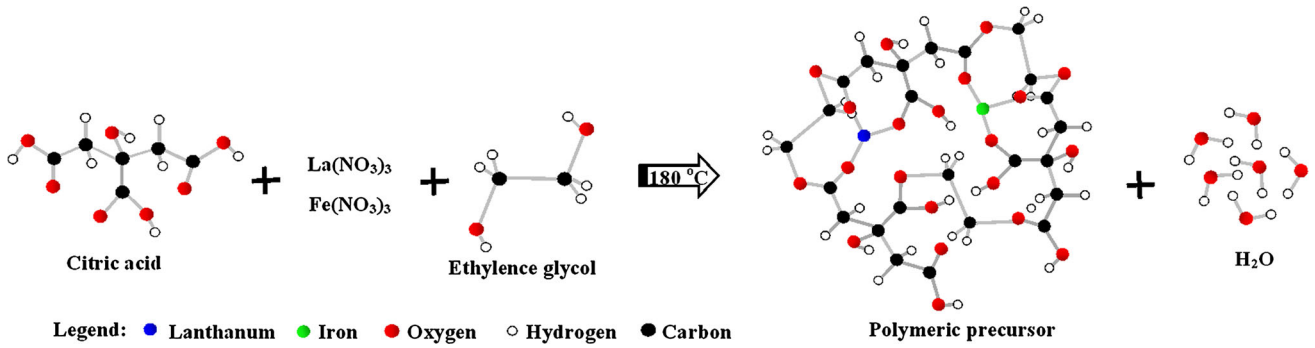

Fig. 1 Schematic representation of polymeric precursor in PC method of $LaFeO_3$ nanoparticles

ethylene glycol (EG) solution. This solution plays an important role to balance the difference in individual behavior of metal ions in solution. It results in a better distribution of ions and prevents the separation of components at later process stages. Initially, the metal ions are introduced into the solution. During the heating reaction, the complexes and production of polymer gel were formed above 100 °C and then the oxidation and pyrolysis of the polymer matrix begin also above 400 °C. This step leads to forming amorphous oxide or carbonate precursor [21]. Therefore, the phase-pure with high-quality $LaFeO_3$ nanocrystalline has been successfully prepared at lower temperature by PC method [22, 23]. This method is suitable in recent years for synthesizing magnetic nano-particles due to the magnetic properties are usually strongly dependent on the particle size.

In this study, the PC method is used to synthesize $LaFeO_3$ nanoparticles and the effect of the particles size on the magnetic properties of $LaFeO_3$ was investigated and discussed. The synthesized $LaFeO_3$ nanoparticles were characterized by thermogravimetric-differential thermogravimetric(TG-DTG), X-ray diffraction (XRD), transmission electron microscopy (TEM), UV–Visible spectroscopy (UV–Vis), X-ray photoelectron spectroscopy (XPS), and X-ray absorption spectroscopy (XAS). The magnetic properties of $LaFeO_3$ nanoparticles were investigated using a vibrating sample magnetometer (VSM) at room temperature (RT).

2 Experimental

In the preparation of $LaFeO_3$ nanoparticles, $LaN_3O_9{\cdot}6H_2O$ (Aldrich), $Fe(NO_3)_3{\cdot}9H_2O$ (Kanto) and $C_6H_8O_7$ (Analar Normapur) were dissolved in EG of 180 ml to promote the polyesterification. The lanthanum (III) and iron (III) ions are bound by the strong ionic bonds between the metallic ions and carboxylate ions in a polymeric chain or between the polymeric chains. The polymeric precursor compound is schematically represented in Fig. 1. The precursor solution

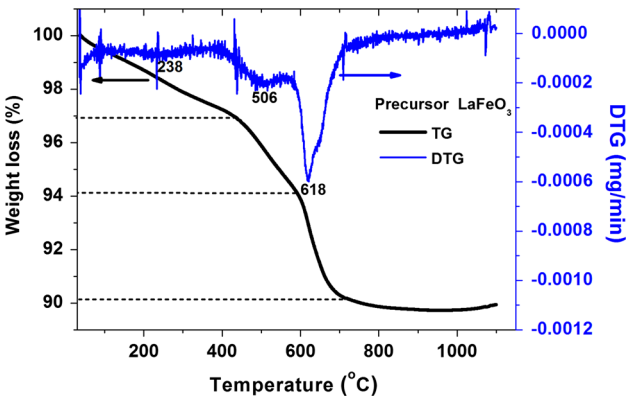

Fig. 2 TG-DTG curve of $LaFeO_3$ precursor

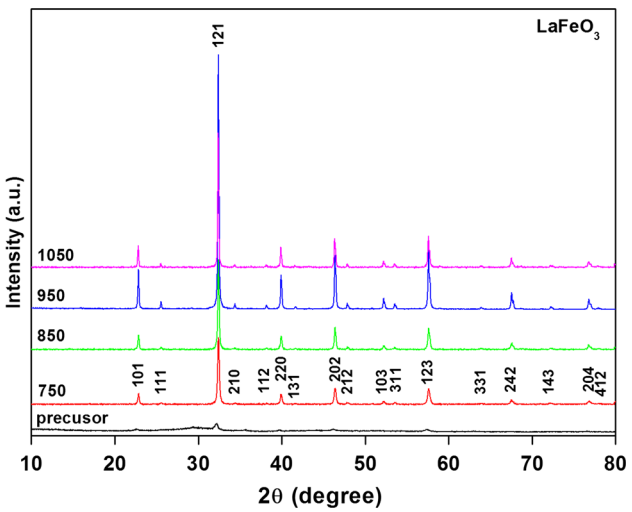

Fig. 3 XRD patterns of precursor and $LaFeO_3$ samples calcined at various temperatures for 2 h in air

was stirred at RT for 6 h and then heated at 180 °C until dried. Then the final product was pre-calcined in a furnace at 400 °C for 2 h, leading to the partial decomposition of the polymeric gel. The precursor was calcined at 750, 850, 950 and 1,050 °C for 2 h in air to obtain single phase.

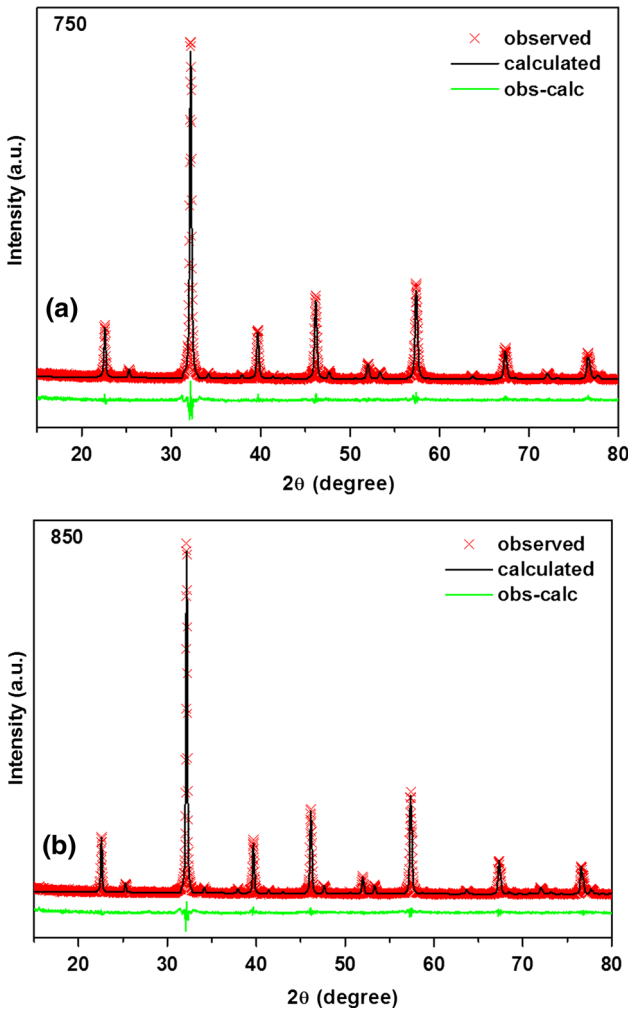

Fig. 4 Refined XRD patterns of $LaFeO_3$ samples calcined at **a** 750 °C and **b** 850 °C. The experimental data are indicated by the *dots* and the calculated data by the *solid line* overlaying them and the *bottom curve* shows the difference between the experimental and calculated data

The prepared samples were characterized using TG-DTG, XRD, TEM, UV–Vis, XPS, XANES, and VSM. Thermogravimetric-differential thermogravimetric analysis (Mettler Toledo Stare System TG-DSC), and X-ray diffractometer (XRD) using Cu Kα radiation with $\lambda = 0.154184$ nm (Bruker D2 Phaser, Germany) were used to study the phases of the $LaFeO_3$ samples. The morphology and crystal structure of the samples were performed using TEM (FEI, TECNAI G^2 20, Netherlands). UV–Vis was performed using a UV-3101PC UV–Vis-NIR scanning spectrometer (Shimadzu, Japan). XPS analysis was performed by AXIS Ultra DKD (Kotros analytical Ltd, Manchester, United Kingdom). The samples were excited with X-ray hybrid mode of monochromatic Al $K_{\alpha 1,2}$ radiation at 1.4 keV. XANES spectra of Fe *K* edge was studied using X-ray absorption near edge spectroscopy in transmission mode at the BL5.2 line at Siam Photon (Synchrotron Research Institute) in Nakhon Ratchasima, Thailand. The magnetic measurements were performed at RT using a vibrating sample magnetometer (VSM, Versa Lab, Quantum Design, USA).

3 Results and discussion

The thermal decomposition and crystallization temperature of the $LaFeO_3$ precursor were obtained by TG-DTG analysis as shown in Fig. 2. The TG curve showed three steps of weight loss between 30 and 1,100 °C. The weight of the sample remained constant at around 700 °C until the temperature up to 1,100 °C, indicates that the reaction is complete and no evidence of a phase transition is present in the sample. On the DTG curve, three peaks were observed at ~238, 506 and 618 °C, suggesting that the thermal events related to the burn-out of moisture and trapped solvent (water and carbon dioxide), and nitrates corresponding reaction of $LaCO_3OH$ into $La_2O_2CO_3$, and $La_2O_2CO_3$ with Fe_2O_3 into $LaFeO_3$ [24].

Figure 3 shows the XRD patterns of the precursor and $LaFeO_3$ samples calcined at various temperatures. The precursor showed amorphous with some weak peak of orthorhombic phase. With increasing the temperature to 750 °C, the diffraction peaks become stronger and sharper, indicating crystallinity of $LaFeO_3$ becomes better during the calcination process. The calcined samples exhibited peaks consistent with the orthorhombic structure of $LaFeO_3$ in the standard from JCPDS 88-0641 and no diffraction peaks corresponding to impurity phases were observed. The Rietveld analysis confirmed a single phase orthorhombic structure (space group Pnma (62)) without any impurity phase. Figure 4a, b show the Rietveld refined plot of the samples

Table 1 Crystallite sizes from XRD line broadening, lattice parameter (*a*, *b* and *c*) calculated from Rietveld refined XRD patterns, and magnetization *M* of $LaFeO_3$ nanoparticles calcined in air at 750, 850, 950 and 1,050 °C for 2 h

Sample	Rietveld refinement						*M* (emu/g)
	Crystallite size (nm)	Lattice parameter (nm)			χ^2	R_{ex} (%)	
		a	*b*	*c*			
750	44.5 ± 2.4	0.5562(6)	0.7856(1)	0.5556(9)	1.190	11.38	0.10
850	55.6 ± 2.9	0.5563(4)	0.7854(6)	0.5555(5)	1.367	11.78	0.08
950	66.2 ± 4.0	0.5565(3)	0.7859(5)	0.5559(3)	1.964	9.81	0.08
1,050	74.1 ± 4.9	0.5563(2)	0.7854(3)	0.5557(2)	1.823	10.78	0.09

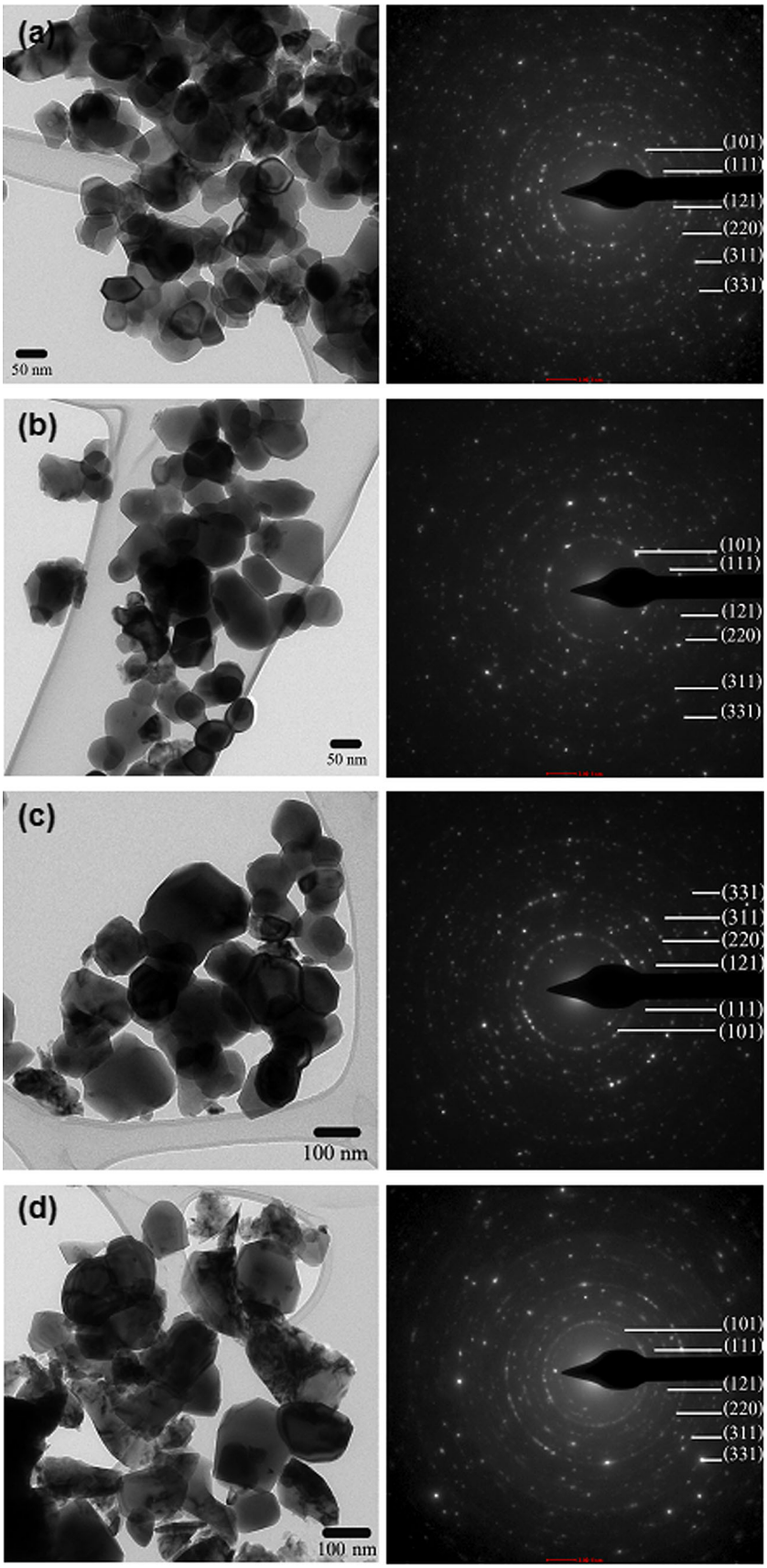

Fig. 5 TEM images with SAED patterns of the $LaFeO_3$ samples calcined at **a** 750 °C, **b** 850 °C, **c** 950 °C and **d** 1,050 °C

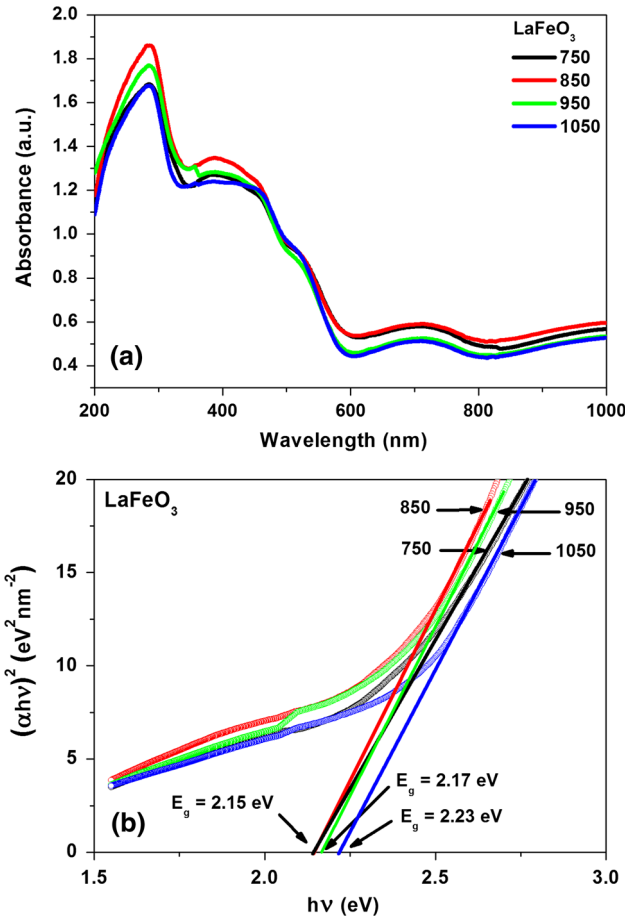

Fig. 6 **a** Room-temperature optical absorbance spectra of the $LaFeO_3$ samples **b** plot of $(\alpha h\nu)^2$ as a function of photon energy for $LaFeO_3$ nanoparticles

calcined at 750 and 850 °C, respectively. The final values for the quality factors and convergence are listed in Table 1. The average crystallite sizes of all samples were calculated from X-ray line broadening of the peaks at (101), (121), (220), (202), and (123) planes using Scherrer's equation. The crystallite sizes were obtained to be 44.5 ± 2.4, 55.6 ± 2.9, 66.2 ± 4.0, and 74.1 ± 4.0 nm for the samples calcined at 750, 850, 950 and 1,050 °C, respectively, which increased with the increase in the calcination temperature. The values of the lattice parameter (a, b, c) were in good agreement with that of orthorhombic $LaFeO_3$ (JCPDS 88-0641) with $a = 0.5564$ nm, $b = 0.7855$ nm, $c = 0.5556$ nm.

The TEM images with selected area electron diffraction (SAED) patterns of the $LaFeO_3$ samples are shown in Fig. 5. The samples showed small nanoparticles with particle size below 100 nm except for the sample calcined at 1,050 °C. Particle size of the sample 950 °C-calcined clearly shows that particles become larger as the calcination temperature increases, which agree with the XRD results. The SAED patterns of the samples showed spotty ring patterns indicative of a polycrystalline structure, which agree with the XRD results.

Figure 6a shows the UV–Vis absorption spectra of the $LaFeO_3$ nanoparticles. All samples showed a strong absorption in the ultraviolet (~200–400 nm) and visible light region (~400–800 nm). This absorption is interesting because $LaFeO_3$ could be developed a new visible light photocatalyst. The direct band gap energy (E_g) was determined by fitting the absorption data to the direct transition as equation $\alpha h\nu = A(h\nu - E_g)^{1/2}$, where α is the optical absorption coefficient, $h\nu$ is the photon energy, E_g is the direct band gap, and A is a constant [25]. The extrapolation of the linear portions of the curves toward absorption equal to zero ($y = 0$) gives E_g for direct transitions (see Fig. 6b). The estimated direct band gaps of all samples were in the range of 2.15–2.23 eV. These band gaps are closed to the values reported in the literature for $LaFeO_3$. For examples, Parida et al. [15] and Yang et al. [26] have reported direct band gap value of 2.1 eV for $LaFeO_3$ nanoparticles synthesized by sol–gel auto-combustion method. Saad et al. [16] have reported a direct band gap value of 2.15 eV for $LaFeO_3$ nanoparticles prepared by sol–gel combustion method. These small band gaps of $LaFeO_3$ are interesting for application in photocatalytic, sensor materials and electrode material in solid oxide fuel cells (SOFCs) [15, 27–30].

The valence states of La, and Fe in the prepared samples were investigated by XPS, which is more sensitive to surface. The XPS spectra of La3d, Fe2p, and O1s of $LaFeO_3$ nanoparticles for samples calcined at 850 and 1,050 °C were measured at RT as shown in Fig. 7a–c for the sample calcined at 850 °C, and Fig. 7d–f for the sample calcined at 1,050 °C. Figure 7a, d show that the peak position at approximately 833.5–833.6 and 850.3–850.6 eV are assigned to La $3d_{5/2}$ and La $3d_{3/2}$ [15, 31], respectively, indicating that the La ions are in the La^{3+} ions. The Fe peak of the samples included two components of Fe^{3+} (709.9–710.0 and 723.2–723.5 eV) and Fe^{4+} (711.6–711.7 and 724.9–725.2 eV) [15, 32] as shown in Fig. 7b, e. This result indicates that the Fe ions in our $LaFeO_3$ samples are in a mixed of the Fe^{3+} and Fe^{4+} valence state. For O ions in $LaFeO_3$, the samples showed similar peak position of crystal lattice oxygen (O_L) at approximately 529.2–529.3 eV and hydroxyl oxygen (O_H) at approximately 531.3–531.6 eV, indicating that it is attributed to the contribution of La–O and Fe–O in $LaFeO_3$ crystal lattice for the O_L signal [31, 32] as shown in Fig. 7c, f.

To confirm the valence states of La and Fe in the prepared $LaFeO_3$ samples, we performed experiments by measuring the XANES. The XANES spectra at Fe K-edge were measured in transmission mode at RT. Figure 8 shows edge energies of the Fe foil, Fe_3O_4 (Fe^{2+}, Fe^{3+}) standard, Fe_2O_3 (Fe^{3+}) standard, and $LaFeO_3$ samples calcined at different temperature for comparison. The shift

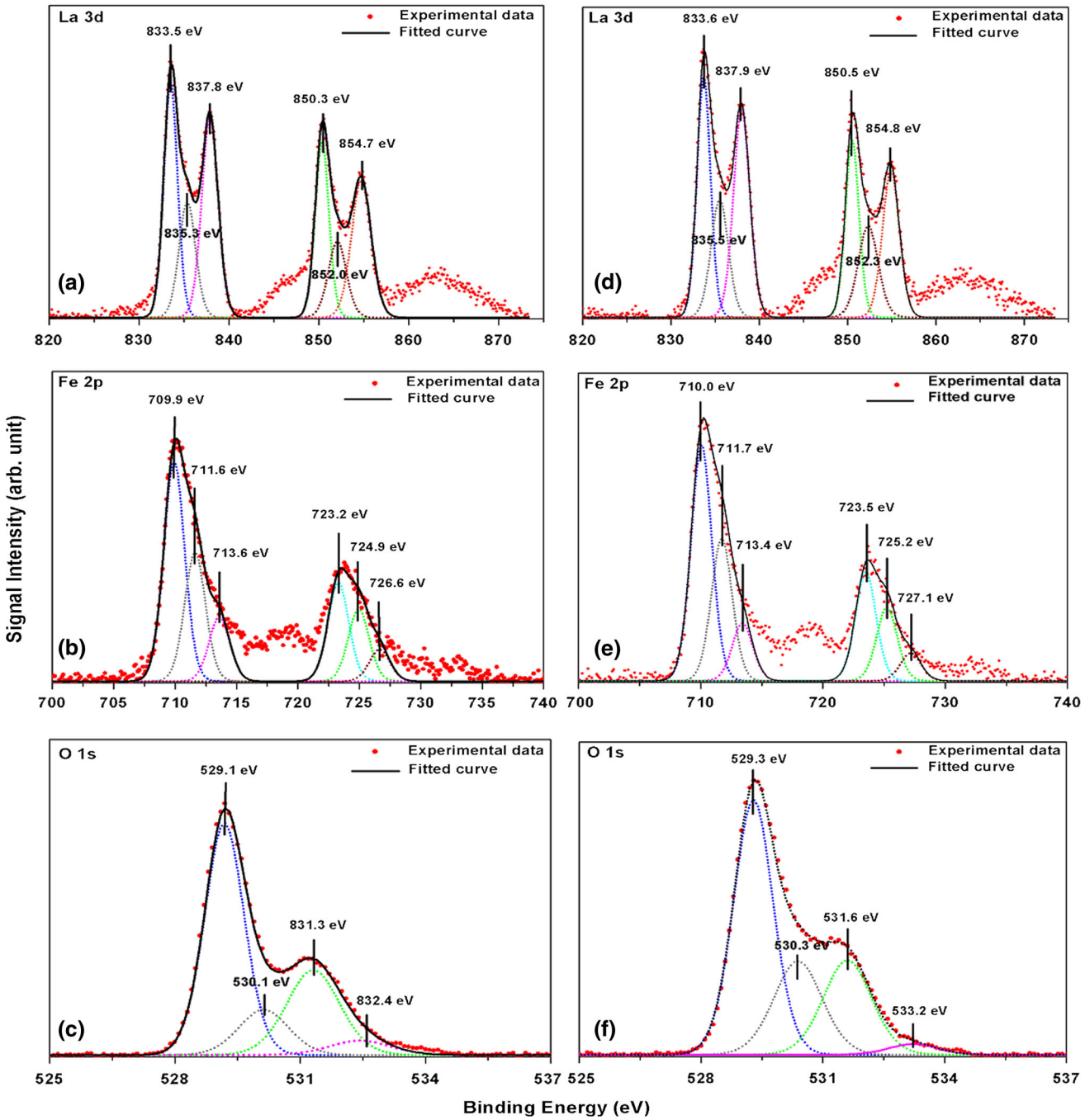

Fig. 7 XPS spectra of La3d, Fe2p and O1s for the $LaFeO_3$ samples calcined at 850 and 1,050 °C

of the edge position can be used to determine the valence state. From Fig. 8, edge position of Fe_3O_4 (Fe^{2+}, Fe^{3+}) standard is approximately 7,124 eV, while Fe_2O_3 (Fe^{3+}) standard is approximately 7,125 eV. In addition, edge position of FeO (Fe^{2+}) standard (as not shown) is approximately 7,120 eV. These can be used simply as a fingerprint of phases and valence state. It is seen that the edge positions of all the samples were upper than those of the Fe^{3+} at approximately 7,126 eV. Thus, this result indicated that most of the Fe ions in our samples are in a mixed valence state of Fe^{3+} and Fe^{4+}, which agree with the XPS results.

The magnetization curves obtained from VSM measurements for all $LaFeO_3$ samples measured at RT with magnetic field (H) in the range of ±10 kOe are shown in Fig. 9. All the $LaFeO_3$ samples exhibit weak ferromagnetic

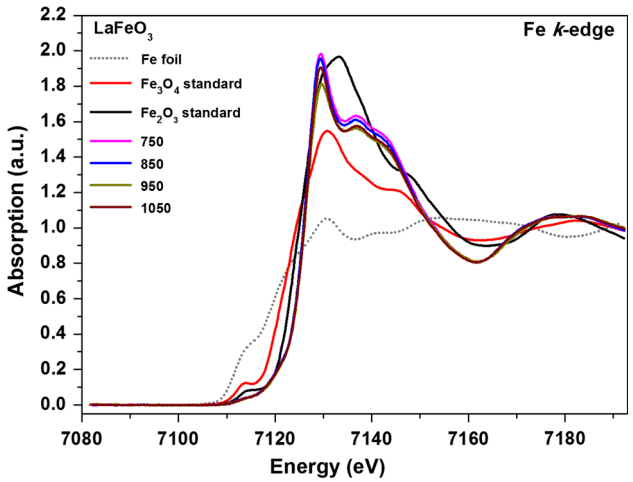

Fig. 8 XANES spectra at the Fe K absorption edge of the Fe foil, Fe_3O_4 (Fe^{2+}, Fe^{3+}) standard, Fe_2O_3 (Fe^{3+}) standard and $LaFeO_3$ samples calcined at different temperatures for comparison

behaviour with the highest magnetization (M) at 10 kOe of ~1.0 emu/g, H_C of ~25–125 Oe. The magnetizations of the $LaFeO_3$ samples in this work are summarized in Table 1. It can be seen that nanoparticles of $LaFeO_3$ show an increase of M with decreasing nanoparticle size as 44.5 ± 2.4 nm in size. This result is of great interest because bulk $LaFeO_3$ is antiferromagnetic behavior due to the superexchange interactions between these neighboring Fe^{3+} ions of Fe^{3+}–O^{2-}–Fe^{3+}. The origin of ferromagnetism in our $LaFeO_3$ nanoparticles could be a result of several reasons. The first possibility is because of the large fraction of uncompensated spins from the surfaces of the nanocrystals and the canted internal spin. This behavior has been also observed in other perovskites $LaFeO_3$ samples as well as in $BiFeO_3$ [33, 34] and $YFeO_3$ [35]. Therefore, for ferromagnetism in perovskites oxides, the small crystallite size is also important consideration because of the increase in surface area. The second is the double exchange (DE) interaction, which is often reported for several oxides. In this work, the XPS and XANES results show the evidence of Fe^{3+} and Fe^{4+} ions in $LaFeO_3$, which can be attributed to the mechanism of Fe^{3+}–O^{2-}–Fe^{4+} ions for DE interaction. Therefore the RT-FM in these samples is suggested as being a result of the FM according to the DE. Finally, ferromagnetism may be originated by TM clusters such as Fe, FeO or Fe_2O_3. Fe is a well-known ferromagnetic material, as FeO (T_N ~ 200 K) and Fe_2O_3 (T_C ~ 240 K) show antiferromagnetic or weak ferromagnetic behavior at low temperature [36]. Our FM results are not from the presence of TM metal clusters because if TM clusters exist

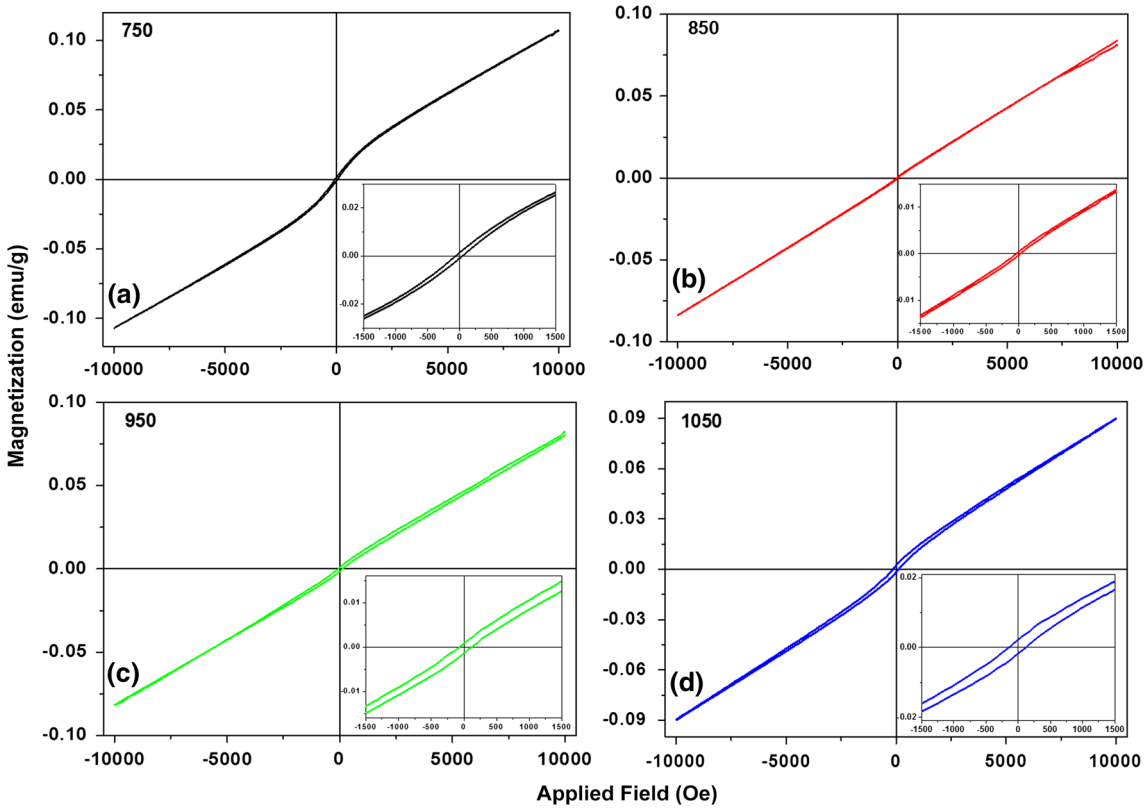

Fig. 9 M–H curves at ±10 kOe measured at RT of the $LaFeO_3$ samples

the magnetic moment would be proportional to the amount of TM concentration. In comparison to other works, the M value of 0.1 emu/g in this work is lower than the value of 0.38 emu/g for $LaFeO_3$ nanoparticles ($\sim$21.9 nm) synthesized by sol–gel reported by Saad et al. [16], the value of 0.44 emu/g for $LaFeO_3$ nanoparticles ($\sim$50 nm) synthesized by milling method reported by Thuy et al. [18], and the value of 0.9 emu/g for $LaFeO_3$ nanofibers ($\sim$20 nm) synthesized by electrospining reported by Lee et al. [37]. The difference in M of $LaFeO_3$ materials depends on the preparation conditions or size of nanoparticles or surface of the nanoparticles. However, further work is needed to study on the bond length and bond angle between Fe and O, and this will be of great interest to understand the ferromagnetic coupling on the DE mechanism.

4 Conclusions

$LaFeO_3$ nanoparticles have been successfully prepared by PC method. Structural characterization showed that the structure had a single phase of orthorhombic $LaFeO_3$. The nanoparticles consisted of the particles of approximately 44.5 ± 2.4–74.1 ± 4.9 nm. UV–Vis spectra showed the prepared $LaFeO_3$ nanoparticles having a strong UV-light absorption. XPS and XANES spectra further confirmed the main composition of the Fe ions were in mixed valence states of Fe^{3+} and Fe^{4+}. Study of magnetic properties at RT showed that $LaFeO_3$ samples with the smallest particle of 44.5 ± 2.4 nm exhibited soft ferromagnetic behavior with magnetization at 10 kOe of $\sim$0.1 emu/g. This behavior indicated that ferromagnetism is due to the uncompensated spins at the surface and the canted internal spin, which is the nature of size-induced magnetism on nanoparticles.

Acknowledgments The authors would like to thank the Synchrotron Light Research Institute (Public Organization), Nakhon Ratchasima, Thailand for XANES facilities, and the Department of Physics, Khon Kaen University for providing VSM facilities. This work is supported by Suranaree University of Technology (SUT) and by the Office of the Higher Education Commission under NRU project of Thailand.

References

1. Tugova EA, Popova VF, Zvereva IA, Gusarov VV (2006) Phase diagram of the $LaFeO_3$–$LaSrFeO_4$ system. Glass Phys Chem 32:674–676
2. Petrovic S, Terlecki A, Karanovic L, Kirilov-Stefanov P, Zduji M, Dondur V, Paneva D, Mitov I, Rakic V (2008) $LaMO_3$ (M = Mg, Ti, Fe) perovskite type oxides: preparation, characterization and catalytic properties in methane deep oxidation. Appl Catal B Environ 79:186–198
3. Tijare SN, Joshi MV, Padole PS, Mangrulkar PA, Rayalu S, Labhsetwar NK (2012) Photocatalytic hydrogen generation through water splitting on nano-crystalline $LaFeO_3$ perovskite. Int J Hydrogen Energy 37:10451–10456
4. Wei Z, Xu Y, Liu H, Hu C (2009) Preparation and catalytic activities of $LaFeO_3$ and Fe_2O_3 for HMX thermal decomposition. J Hazard Mater 165:1056–1061
5. Faye J, Bayleta A, Trentesauxb M, Royera S, Dumeignil F, Duprez D, Valange S (2012) Influence of lanthanum stoichiometry in $La_{1-x}FeO_{3-\delta}$ perovskites on their structure and catalytic performance in CH_4 total oxidation. J Appl Catal B 126:134–143
6. Bellakki MB, Kelly B, Manivannan V (2010) Synthesis and characterization and property studies of (LaAg)FeO_3 perovskite materials. J Alloys Compd 489:64–71
7. Andoulsin R, Horchani-Naifer K, Férid M (2013) Electrical conductivity of $La_{1-x}Ca_xFeO_{3-\delta}$ solid solutions. Ceram Int 39:6527–6531
8. Karpinsky DV, Troyanchuk IO, Sikolenko V, Efimov V, Kholkin AL (2013) Electromechanical and magnetic properties of $BiFeO_3$–$LaFeO_3$–$CaTiO_3$ ceramics near the rhombohedral-orthorhombic phase boundary. J Appl Phys 113:187218
9. Rajendran M, Bhattacharya AK (2006) Nanocrystalline orthoferrite powders: synthesis and magnetic properties. J Eur Ceramic Soc 26:3675–3679
10. Kodama RH, Makhlouf SA, Berkowitz AE (1997) Finite size effects in antiferromagnetic NiO nanoparticles. Phys Rev Lett 79:1393
11. Winkler E, Zysler RD, Mansilla MV, Fiorani D (2005) Surface anisotropy effects in NiO nanoparticles. Phys Rev B 72:132409
12. Kodama RH, Berkowitz AE (1999) Atomic-scale magnetic modeling of oxide nanoparticles. Phys Rev B 59:6321
13. Rajagukguk R, Shin DG, Lee BW (2011) Magnetic ordering in $(1-x)BaTiO_3$–$xLaFeO_3$ solid solutions. J Magnetics 16(2): 101–103
14. Liu T, Xu Y (2011) Synthesis of nanocrystalline $LaFeO_3$ powders via glucose sol–gel route. Mater Chem Phys 129:1047–1050
15. Parida KM, Reddy KH, Martha S, Das DP, Biswal N (2010) Fabrication of anocrystalline $LaFeO_3$: an efficient sol–gel autocombustion assisted visible light responsive photocatalyst for water decomposition. Int J Hydrogen Energy 35:12161–12168
16. Saad AA, Khan W, Dhiman P, Naqvi AH, Singh M (2013) Structural, Optical and magnetic properties of perovskite $(La_{1-x}Sr_x)(Fe_{1-x}Ni_x)O_3$, (x = 0, 0.1, 0.2) nanoparticles. Electron Mater Lett 9:77–81
17. Kumar M, Srikanth S, Ravikumar B, Alex TC, Das SK (2009) Synthesis of pure and Sr-doped $LaGaO_3$, $LaFeO_3$ and $LaCoO_3$ and Sr, Mg-doped $LaGaO_3$ for ITSOFC application using different wet chemical routes. Mater Chem Phys 113:803–815
18. Thuy NT, Minh DL (2012) Size effect on the structural and magnetic properties of nanosized perovskite $LaFeO_3$ prepared by different methods. Adv Mater Sci Eng 1155:380306
19. Sivakumar M, Gedanken A, Zhong W, Jiang YH, Du YW, Brukental I, Bhattacharya D, Yeshurun Y, Nowik I (2004) Sonochemical synthesis of nanocrystalline $LaFeO_3$. J Mater Chem 14:764–769
20. Zheng WJ, Liu RH, Peng DK, Meng GY (2000) Hydrothermal synthesis of $LaFeO_3$ under carbonate-containing medium. Mater Lett 43:19–22
21. Kakihana M (1996) "Sol–Gel" preparation of high temperature superconducting oxides. J Sol-Gel Sci Technol 6:7–55
22. Popa M, Frantti J, Kakihana M (2002) Lanthanum ferrite $LaFeO_{3+d}$ nanopowders obtained by the polymerizable complex method. Solid State Ionics 154–155:437–445
23. Popa M, Frantti J, Kakihana M (2002) Characterization of LaMeO3 (Me: Mn Co, Fe) perovskite powders obtained by polymerizable complex method. Solid State Ionics 154–155:135–141

24. Kaiwen Z, Xuehang W, Wenwei W, Jun X, Siqi T, Sen L (2013) Nonacrystalline $LaFeO_3$ preparation and thermal process of precursor. Adv Powder Technol 24:359–363
25. Ziegler E, Heinrich A, Oppermann H, Stover G (1981) Electrical properties and non-stoichiometry in ZnO single crystals. Phys Status Solidi A 66:635–648
26. Yang Z, Huang Z, Ye L, Xie X (1999) Influence of parameters U and J in the LSDA+U method on electronic structure of the perovskites LaMO3 (M = Cr, Mn, Fe Co, Ni). Phys Rev B 60:15674–15682
27. Koferstein R, Jager L, Ebbinghaus SG (2013) Magnetic and optical investigations on $LaFeO_3$ powders with different particle sizes and corresponding ceramics. Solid State Ionics 249–250:1–5
28. Tang PS, Fu MB, Chen HF, Cao F (2011) Synthesis of nanocrystalline $LaFeO_3$ by precipitation and its visible-light photocatalytic activity. Mater Sci Forum 694:150–154
29. Song P, Quin H, Zhang L, An K, Lin Z, Hu J, Jiang M (2005) The structure, electrical and ethanol-sensing properties of $La_{1-x}Pb_xFeO_3$ perovskite ceramics with $x \leq 0.3$. Sensors Actuat B Chem 104:312–316
30. Bidrawn F, Lee S, Vohs JM, Gorte RJ (2008) The effect of Ca, Sr, and Ba doping on the ionic conductivity and cathode performance of $LaFeO_3$. J Electrochem Soc 155:B660–B665
31. Thirumalairajan S, Girija K, Ganesh V, Mangalaraj D, Viswanathan C, Ponpandian N (2013) Novel synthesis of $LaFeO_3$ nanosructure dendrites: a systematic investigation of growth mechanism, properties, and biosensing for highly selective determination of neurotransmitter compounds. Cryst Growth Des 13:291–302
32. Wei ZX, Wang Y, Liu JP, Xiao CM, Zeng WW, Ye SB (2013) Synthesis, magnetization, and photocatalytic activity of $LaFeO_3$ and $LaFe_{0.9}Mn_{0.1}O_{3-\delta}$. J Mater Sci 48:1117–1126
33. Mazumder R, Ghosh S, Mondal P, Bhattacharya D, Dasgupta S, Das N, Sen A, Tyagi AK, Sivakumar M, Takami T, Ikuta H (2006) Particle size dependence of magnetization and phase transition near T_N in multiferroic $BiFeO_3$. J Appl Phys 100:033908
34. Gao F, Yuan Y, Wang KF, Chen XY, Chen F, Liu JM, Ren ZF (2006) Preparation and photoabsorption characterization of $BiFeO_3$ nanowires. Appl Phys Lett 89:102506
35. Maiti R, Basu S, Chakravorty D (2009) Synthesis of nanocrystalline $YFeO_3$ and its magnetic properties. J Magn Magn Mater 321:3274–3277
36. Phokha S, Pinitsoontorn S, Maensiri S (2012) Structure and magnetic properties of monodisperse Fe^{3+}-doped CeO_2 nanospheres. Nano-Micro Lett 5(4):223–233
37. Lee WY, Yun HJ, Yoon JW (2014) Characterization and magnetic properties of $LaFeO_3$ nanofibers synthesized by electrospining. J Alloy Compd 583:320–324